



Nano-architecture of CaO/Ag-chitosan nanocomposite by sol gel process: formation and characterization



CrossMark

Amany M. El Nahrawy^{1*}, Ahmed M. Bakr², Ali B. Abou Hammad¹, A. M. Mansour¹

¹Solid State Physics Department, Physics research division, National Research Centre, 33 El Bohouth St., Dokki, Giza 12622, Egypt.

²Spectroscopy Department, Physics Research Division, National Research Centre, 33 El Bohouth St., Dokki, Giza, 12622, Egypt

Abstract

Functionalize nano-architecture CaO/Ag-chitosan bio-nanoparticles were prepared by the acetic acid sol-gel process and were loaded into the chitosan nanocomposite. The so prepared bioactive nano-CaO/Ag-chitosan nanocomposite was characterized using XRD, TEM, FE-SEM, optical, and the antimicrobial activity was evaluated. The antibacterial evaluations implied that chitosan, nano-CaO, and nano-CaO/Ag-chitosan are exhibited subtle antimicrobial activities against both Gram-positive (*Staphylococcus aureus*) microbes and Gram-negative (*Escherichia coli*). Ag doping of CaO produces an oxygen vacancy, defects, and improved light scattering and so leads to transmission increase and absorption increase which in turn lead to increase of the bandgap energy. The optical conductivity of the nanocomposites decreased with Ag addition as a direct result of the bandgap increase. These prefatory investigations of the bio nanocomposites will open a good platform for their use in various bio-industries.

Keywords: Chitosan–CaO; Ag nanocomposites; Sol-gel process; Optical; Antimicrobial.

1. Introduction

Metal oxide (MO) nanoparticles have recently gotten a lot of interest because of their potential applications in optoelectronics, catalysts, adsorbents, and bactericides [1–3].

Because of their plentiful supply of raw materials, good thermal stability, low biological toxicity, and bio-degradability, MO nanoparticles have a wide range of applications [4, 5]. Nanostructures metals are a course of functional materials that have discrete physical and chemical properties that are subjective by their relative composition, scale, and structure. Generally, metal structures nano-sized have distinctive optical properties which makes them an ideal applicant for numerous applications [1].

Metal-organic composite (M-OC) can be obtained with the optimum combination of the high molecular, high oxidation resistance, and low density of the organic and the hardness of the metal oxides [6, 7]. Therefore, the M-OCs are accredited as applicants for water treatment, sensors, biomaterials, and catalysts applications [8, 9]. The use of metal oxide nanoparticles for drug delivery and water treatment is getting a lot of attention now [10, 11].

As photocatalysts, metal oxides are desirable because of their cost-effectiveness, reliability, recyclability, and environmental friendliness [12]. The operation of metal oxides as an active photocatalytic is significantly improved by their structural compositions and surface defects. This due to that the doping of metal oxides with metal and/or metals raises surface defects, improves optical and electronic properties, and transfers optical absorption into the visible region [13–15]. To evolve the metal-organic composites as good platforms for various applications, alkaline metal oxides have been well purposed as organic linkers with metal-organic composites because of their excellent structural, catalytic, and antimicrobial activities.

The alkaline earth metal oxides working for the various chemical reaction and transesterification reaction survey the mandate of their activity:- BaO, AgO, CaO, SrO, MgO; ...etc [16–19].

Unique metal oxides either establish low activity and/or leaked out into the reaction combination to cause the uniform contribution in the catalytic activity [16]. To improve both the reactivity well as stability, mixed metal oxides of various alkali earth

*Corresponding author e-mail: amany_physics_1980@yahoo.com; (Amany M. El Nahrawy).

Receive Date: 14 June 2021, Revise Date: 25 June 2021, Accept Date: 04 July 2021

DOI: 10.21608/EJCHEM.2021.80608.3995

©2021 National Information and Documentation Center (NIDOC)

oxides were synthesized and employed for the active chemical reactions. The active centers in the catalysts reactions are either oxide ion or permeated metal oxide or the different defects created because of metal impregnation [16].

Silver is probably considered the most noteworthy material in biological and plasmonics. It offers numerous advantages over Cu, Pd, Au, and other metals to maintenance surface plasmons in the visible and the near-infrared regions of the electromagnetic spectrum [20]. Ag, as related with other metals, is exclusive for its excellent features in terms of available nanostructures, plasmonic ability, conductivity, eco-friendly, and material cost. Silver has the best thermal and electrical conductivity amongst all metals, which makes it an ideal applicant for electrical interconnection. Silver can produce a region of electric field and enhance the electrical properties through surface Plasmon, optical vibration [21].

Ag doping of MO matrix causes oxygen vacancies, crystal faults, and increased light scattering, and all of which lead to an increase of MO NPs' electrical, optical, and photocatalytic performance [1]. Since the radius of Ag^+ (0.126 nm) is greater than that of most other metals, Ag atoms can occupy substitutional instead of interstitial sites if doped within the MO matrix [1]. Furthermore, since Ag dopant has a detrimental effect on metal oxide grain growth [22, 23], Ag doping can result in a reduction in particle size. So, a nanocomposite with smaller particle sizes can be obtained, and then a greater interaction between MO and the whole matrix will exist [1].

Chitosan is one of the abundant bio-polymers is based on their linear bio-polyamines-charge obtained by alkaline deacetylation of chitin [24].

Chitosan (CS) is a promising organic biomedical natural polymer with a variety of applications due to its non-toxicity, water-solubility, cytocompatibility, bio-adhesive, and absorption-enhancing features [25]. CS is solvable through the acidic solutions, and its complete solubility is affected by the degree of the deacetylation, used acid, and the molecular weight to protonate their amino group. CS easily interacts with surfaces with negative charges such as proteins and anionic polysaccharides due to its linear polyelectrolyte chain with a high cationic charge level [19]. The structure of CS is close to that of hyaluronic acid and glycosaminoglycans found in the human body. Because of the abundance of strongly reactive $-\text{NH}_2$ groups, CS is highly vulnerable to chemical functionalization [26]. The CS biocompatibility is asserted by the certainty that it is tainted in vivo by the lysozyme, which yields N-acetylglucosamine, an important constituent of casing keratin protein. Because of its strong aqueous solubility, CS can be made into several structural

types such as nanoparticles, nanofibers, and gels [27]. The aldehyde and hydroxyl groups in the loaded metal sols may form a Master base with the amino group of chitosan and the phenolic hydroxyl might format hydrogen chains with chitosan to found adherence network structures of nano or microspheres [27–29]. A nanocomposite is a type of advanced material that incorporates nanosized particles into the matrix to improve its properties [30]. This is because nanoscale building blocks can be used to develop and produce new materials with unparalleled precision and enhanced properties [6]. Polymer nanocomposites have a variety of uses in recent decades, the majority of which are in the automotive field. In comparison to pure polymer, adding nanoparticles to the polymer matrix improves the properties of the nanocomposites [31].

CaO nanoparticles are one of the successful nano-filler employed in the fabrication of hybrid nanocomposite arrangements, owing to their homogenous nanoparticles size and sizeable penetration within the polymer layers [32]. The chemical polymerization sol-gel route is the strategic technique for the fabrication of films, nanoparticles, and porous ceramics based on inorganic molecules [11, 14, 33]. For fabrication of the chitosan nanocomposite with nano-Ca and nano-Ca/Ag ions-promising properties, the nanofillers should offer a small distribution in diameter size and highly dispersed in the chitosan matrix [34].

This study was expected to develop a nano-CaO-chitosan nanocomposite and loaded with Ag nanoparticles prepared via the acetic acid sol-gel process. The insertion of nano-CaO and nano-CaO/(0.0-0.6 wt.%) Ag into a chitosan matrix using the acetic acid sol-gel is an amended study. Then, the nano-architecture of CaO/Ag-chitosan nanocomposites is characterized with XRD, TEM, and FE-SEM. It is thought that the variation in a surface polarity match between CaO and chitosan can observe the proper bio-compatibility of nano-CaO/Ag NPs with chitosan matrix. Finally, both the optical property and antimicrobial tests of the as-prepared nano-CaO/Ag -chitosan nanocomposites are studied in detail.

2. Experimental work

2.1. Materials

Chitosan (deacetylation degree =90 %, viscosity=50–800 mPa·s; Mw =193 kDa, China) Calcium and silver nitrates ($\text{Ca}(\text{NO}_3)_2$ and AgNO_3) were purchased from Sigma. Acetic acid ($\text{CH}_3\text{CO}_2\text{H}$, Sigma), ethylamine ($\text{C}_2\text{H}_5\text{NH}_2$, $\geq 97.0\%$, Sigma) and Distilled water.

2.2. Preparation of nano-CaO/Ag NPs-chitosan nanocomposites

The nano-CaO/Ag NPs-chitosan composites were prepared by a chemically acetic sol-gel process at 50 °C.

(a) The nano-CaO/(0.0-0.6 wt.%) Ag was prepared at first. Typical amounts of calcium nitrate, silver nitrate, and acetic acid were dissolved in the used solvent of ethylamine (20 mL) distilled water (25 mL) under magnetic stirring for 35 min at 50 °C. Then the nano-CaO and nano-CaO/Ag sols were aged into dark glass potters at 50 °C for 24 h before insertion into the chitosan matrix.

(a) 3 g chitosan was dissolved in 150 mL of distilled water/ 5 mL acetic acid under vigorous stirring at 50 °C, followed by adding 0.6 mL of freshly prepared nano-CaO sol under magnetic stirring for 30 min. Then, the formation of nano-CaO-(0.2-0.6)Ag was loaded in the chitosan matrix at 50 °C. Upon, the addition of Ag NPs, the reaction mixture was converted to a nearly unclear yellow color, indicating the formation of nano-CaO/Ag NPs-chitosan composite. After the continuous stirring for 30 min, the solution was cooled to room temperature and casting in Petri dishes. Finally, the prepared nanocomposites were dried at 50 °C, washed with distilled water, and dried at 50 °C for 15 min.

2.4. Characterization

X-ray diffraction (XRD, MPDDY-2094, Netherlands) measurement was used to study the phase assembly of the nano-architecture of CaO/Ag-chitosan nanocomposites samples, performed on an X-ray diffractometer at (30 kV and 25 mA) with copper (K α at $\lambda = 1.5406$ nm). The occurrence of phases has been branded with the JCPDS data files in Pcpdfwin-software.

Transmission electron microscopy (TEM) was willful at a quicker voltage of [200 kV] by transmission electron microscopy using (Tecnai(F20 S)-Twin). The nanocomposites were isolated in ethanol/ glycerin (1:1), and small droplets of suspensions were placed on the carbon-coated copper grids for direct observation.

Scanning electron microscopy (SEM) images were passed out through a Philips [EM 420 (200 kV)] to investigate the local surface morphology. The samples were placed in the specimen holder, sputter-coated with a thin layer of gold, and checked using a scanning electron detector at an accelerated voltage of 15 kV.

The optical reflectance and transmission spectra were considered by a Jasco V-570 spectrophotometer over the wavelength range (0.2-2.5 μ m). Refractive index (n) up 500 nm of nano-CaO-chitosan and nano-CaO/Ag-chitosan nanocomposites samples were calculated optically.

Antimicrobial Activity

The antibacterial activity for the prepared nanocomposites was carried out via the agar diffusion method through employed various pathogenic microorganisms such as (*Staphylococcus aureus*) as a model of Gram-positive Bacteria, (*Pseudomonas aeruginosa*) as the model of Gram-negative Bacteria and (*Candida albicans* and *Aspergillusniger*) as models of fungal species. The Antibacterial efficacy media used for the antibacterial testing of the chitosan nanocomposites under study have the following compositions (g/l):- Nutrient agar medium:- peptone 5.0, D-glucose 5.0, NaCl 5.0, meat extract 5.0, and agar 20, pH was adjusted to 7, exerted for the growth of bacterial strains.

Antimicrobial potential Assay

The antibacterial activity of Ag/Ca chitosan nanocomposites was evaluated through the disc diffusion method by using the above test organisms. Ag/Ca chitosan nanocomposite samples were formed into disc shapes of 15 mm diameter and UV sterilized for 2 hours, then placed over the agar surface plates freshly inoculated with the test microorganisms (Nutrient agar medium for bacterial strains). The Petri-dishes were saved in a refrigerator for one hour to authority the homogenous diffusion of the antibacterial agent before the growth of the test microorganisms and then plates were incubated at 37 °C for 24 hours. The surface of the solidified agar plates was allowed to dry in an incubator before the streaking of microorganisms onto the surface of the agar plates. This test was repeated three times. The presence of a clear inhibition zone around the nanocomposite sample in the immunized Petri-dishes is a signal of the antibacterial activity of nano-Ag/Ca chitosan nanocomposite[35–37].

3. Results and discussion

3.1. Electrostatic attraction during acetic sol-gel polymerization

The chemical strategy for making nano-CaO/(0.0-0.6 wt.%) Ag introduced in the nano-CaO-chitosan matrix is offered in Fig.(1). The two-steps chemical procedure was used, outset from the nano-CaO/Ag nanoparticles followed by in-situ polymerization in the chitosan solution.

The loading of nano-CaO and nano-CaO/Ag inside chitosan walls was formed using the in-situ polymerization via the poly-condensation in the acetic sol-gel process. The preparation of nano-CaO and doped with Ag NPs through the formation of covalent and -OH linkages from the reaction of Ca with Ca or Ag in the sol-gel reaction at 50°C [4, 15, 38, 39], as manifested in Fig. 1.

The reactions of Ca and Ca/Ag cross-linking are may be due to the formation of a good cyclic hydrate intermediate between adjacent (Ca-O-Ca-O-OH),

(Ca-O-OH), and (Ca-O-Ag-O-OH) groups in liquid sol as a function of changes in Ag concentrations [40]. Additionally, the introduction of a higher concentration of Ag NPs will lead to ionic substitution by incorporation of Ag atoms in the Ca structure and form ions into the form of Ag-O-Ca and Ca-O-Ag-O-OH. These tendencies in the preparation of various nanoparticles formed by the sol-gel method were reported [41–44].

Generally, the doping method is thought the more effective way to increase and proved highly efficient nanosystems with structural, optical, and bio-responses [25, 45].

Then, the nano-Ca and Ca/Ag sols are familiarized to allow the multi-reactions of the hydroxyl groups of the chitosan as a polysaccharide through their ring-opening and/or the inner-collapses, followed by rearrangement and formation of a homogeneous crosslinking with the elimination -OH groups via the loading Ca and Ca/Ag NPs in chitosan matrix. The chitosan matrix played an essential role in the

formation reaction allows the chemical reduction of Ag, and it similarly served as a good stabilizing agent for nano-Ca/Ag NPs during the polymerization.

Firstly, both nano-Ca and nano-Ag ions were chelated to the (-NH₂) groups into the chitosan chain, and subsequently were formed complex nano-architecture nano-CaO/Ag-chitosan nanocomposites a company with excess of -OH and -NH₂ groups during the polymerization condition, as illustrated in Fig.1.

Herein, Both Ca and Ca/Ag ions are the hydrophilic segments of the surfactant arranged along its chitosan chains, thus, were associated with the elimination of water molecules, and others solvents cover the surfaces of the nanocomposites with hydrophobic segments.

Consequently, the bio nano-CaO NPs were activated by the interactions between the nano-Ca/Ag and the functional groups of chitosan molecules with increasing Ag atoms on the nanocomposite surface.

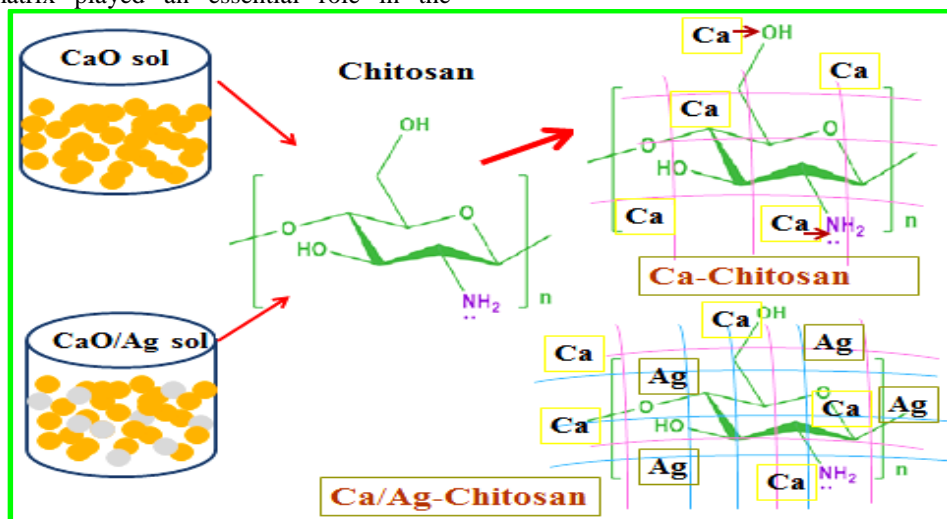


Fig 1. Schematic illustration of the procedure for the preparation of nano-CaO sol and nano-Ca/Ag-chitosan nanocomposites.

3.2. XRD

The crystalline phase of the prepared nano-architecture CaO-chitosan and loaded with (0.4, 0.6 wt%) Ag nanocomposites were predictable by the X-ray diffraction through comparing their X-ray results to the standards with the collective Committee on Powder Diffraction Standards; JCPDS. From the X-ray observation in Fig. 2, the common X-ray pattern of chitosan matrix showing broad peaks for its crystalline nano-CaO-chitosan nanocomposite, nano-architecture CaO-Chitosan nanocomposite, and loaded with (0.4, 0.6 wt%) Ag show broader peaks at $2\theta = 11^\circ, 23^\circ, 32^\circ$ and 42° , indicating higher cross-linkage between chitosan and nano-CaO/Ag and good crystalline phase [18, 39, 46].

The primary crystalline at (32.4°) for CaO was increased upon loading Ag indicating structural ordering [32]. The transformation in XRD spectra for nano-CaO-chitosan undergo the effect of Ag loading can be ascribed to orthorhombic phase- calcium oxide (78-0649) and Chitosan (40-1517). Where the crystalline structure of chitosan-based nanocomposites depends on their degree of deacetylation [47].

Also, when the affine content of nano-CaO is supported with Ag NPs within the chitosan matrix, the evaporation of -OH and solvents results in a higher degree of semi-crystallization of the formed phases. It is observed that semi-crystalline phases of the CaO-chitosan nanocomposites the internal structure with amorphous structure trend were in agreement with reported modified chitosan-based systems [48–50].

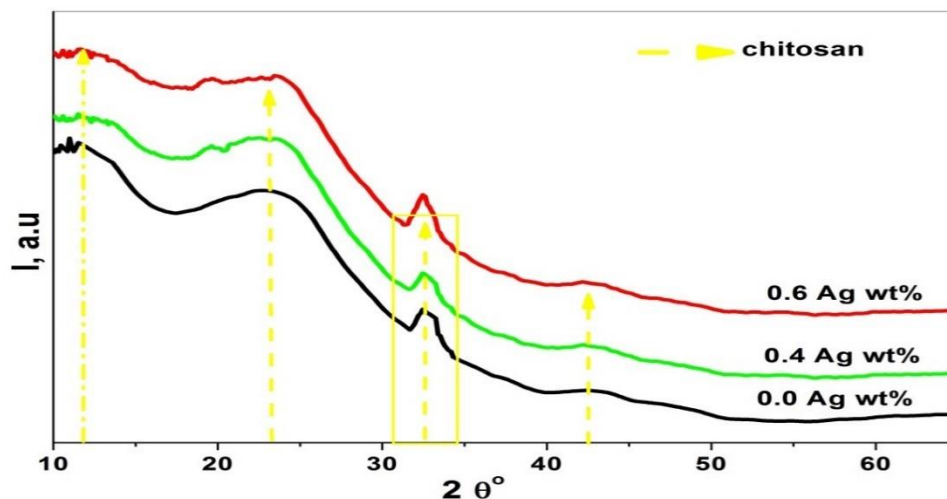


Fig. 2. XRD spectra of nano-CaO-chitosan nanocomposite loaded with Ag NPs.

3.3. TEM/SEM

Both pure nano-CaO-chitosan and loaded with nano-CaO-0.4 Ag-chitosan are chosen as the two representative samples to study the morphological characteristics by TEM and Fe- SEM, as manifested in Fig. (3). The main evidence of the internal structure of nano-CaO and nano-CaO- 0.4 Ag into chitosan polymer matrix are confirmed with TEM images Fig. 3(a, b), which are appears the existence of Ca and Ca/Ag nanoparticles. Fig. 3(a, b) seen that the formed sol-gel Ca and Ca/Ag NPs are uniformly dispersed in the entire chitosan matrix with a spherical shape. Also, there is some nano-Ca/Ag NPs agglomeration is observed in the TEM images.

The two FE-SEM images of the nano-architecture CaO-chitosan without Ag and with 0.4 Ag are manifested in Fig. 3 (c, d) at 15 Kv. The micrographs of the two nanocomposites samples confirmed the smooth and homogeneous intromission of nano-CaO and nano-CaO/0.4 Ag into the graft chitosan biopolymer matrix with the fine distribution.

3.4. Optical discussion

As stated by the band principles of solids, only discrete energy levels are possible for electrons in isolated atoms, but after the atoms are got alongside as in crystalline materials, such degenerate energy states are modified to many individual levels on account of atomic connection. Since the levels are so tightly segregated, they could be viewed as a continuous band of allowable energy states. The two bands with the top energy are the valence band and the conduction band. These bands are apart by a zone that

shows the prohibited energy levels in the solid known as the gap or bandgap[51]. It also shows the energy change among the optimum energy of the valence band and the minimum energy of the conduction band. The energy of the forbidden band can be determined by measuring the absorption of light as a function of the energy of the photon ($h\nu$) [52]. Light is only strongly absorbed if it is greater than the energy gap. The energy from the absorbed photons is used to create a pair of electrons and holes. If $h\nu$ is lowered below the energy gap, the sample becomes transparent to light [53].

The measured transmittance (T) and the reflectance of the samples are presented in Fig. 41. It shows that the transmittance nearly didn't affect by wavelength change. The addition of Ag ions leads to an increase in transmittance. The addition of 0.4 Ag led to an increase of it by about 7 times from its original value. However, at the same time the reflectances (R) exhibit a neglected value with no change by wavelength change. Semiconductors doping with gold (Au), palladium (Pd), silver (Ag), etc. gets a significant outcome on their photoactivity[54]. Silver (Ag) doping is the most effective choice to obtain the demanded benefits due to its strength to develop an electric field site and boosted electrical properties through surface Plasmon optical vibration [54]. Ag doping produces a vacancy (oxygen vacancy), defects, and improved light scattering that increase the efficiency of photoactivity of semiconducting nanoparticles[54].

Accordingly, the absorption coefficient (α) can be calculated from the measured T and R values [55].

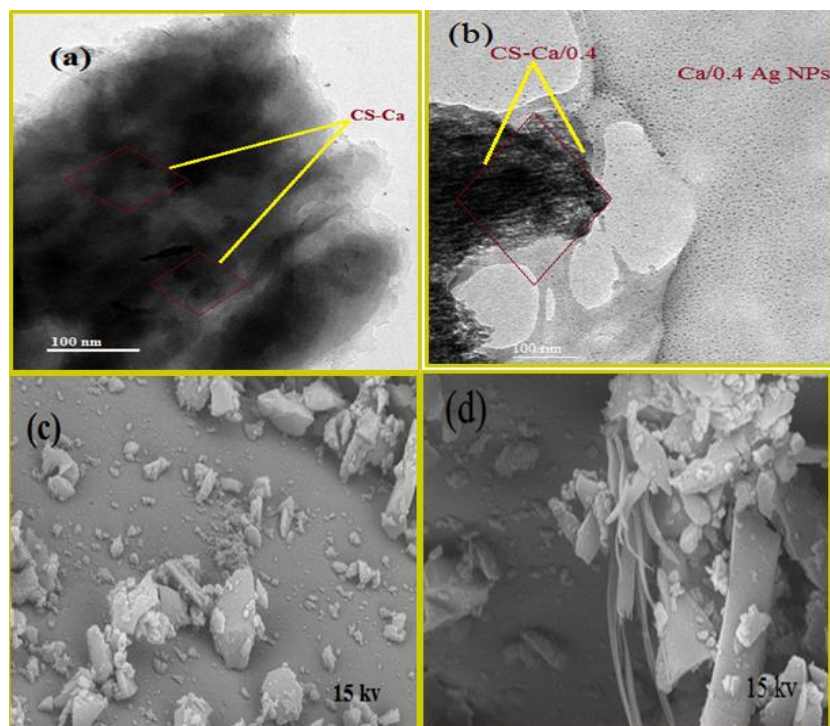


Fig. 3. TEM images of (a) nano-CaO-chitosan, (b) nano-CaO/0.4 Ag-chitosan and (c, d) FE-SEM at 15 Kv for the same samples.

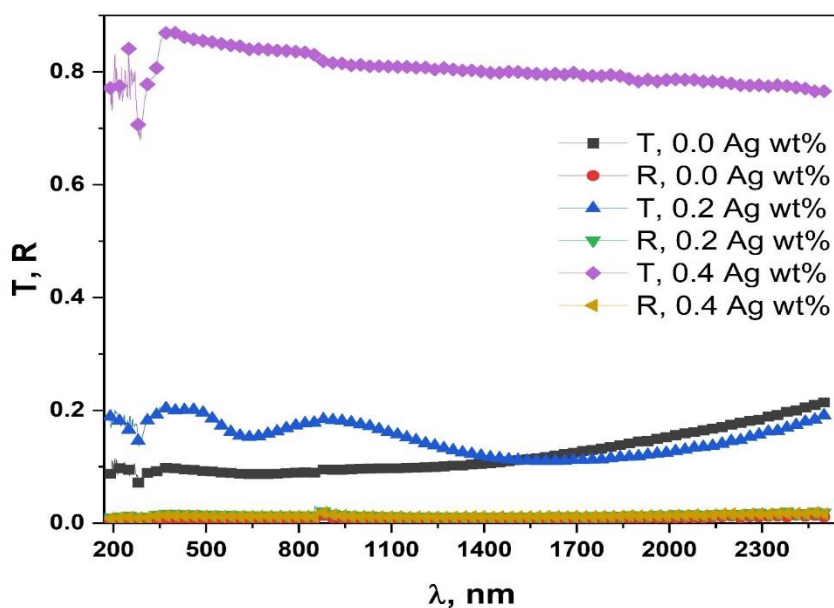


Fig. 4. Transmittance and the reflectance spectra of nano-CaO-chitosan and loaded with Ag-NPs.

The absorption coefficient (α) specifies how much light of a given wavelength can pass into a substance before being absorbed. The absorption coefficient is determined by the substance as well as the wavelength of energy absorbed. For all of the films analyzed, the absorption coefficient was measured at the absorption

edge at varying photon energies and known the thickness (d) employing the next formula [56]:

$$\alpha = (1/d) \ln((1 - R)^2 / T)$$

The absorption coefficient, Fig. 5 (a), shows a value decrease with Ag addition. An absorption peak is observed at about 284 nm and it slightly shifts to a lower wavelength with Ag addition, i.e. shifted to 281 and 279 nm with the addition of 0.2 and 0.4 wt.% Ag.

This shift in absorption peak position is attributed to the addition of Ag in the composite matrix [57]. This will lead to an increase of the nanocomposites bandgap with Ag addition as shown in Fig. 5(a, b (I, ii, iii, and v)) [57].

This increase of the optical bandgap of the composites with silver incorporation is owing to the induced bandgap renormalization effect [58]. The renormalization of the bandgap is developed because of the happened exchange interaction (sp-d) in-band electrons and contained d-electrons of (Ag⁺) [54]. After the promising exchange interaction, there will

be a modification in the bandgap of Ag-doped composites concerning pure one [54]. Lopez-Badillo et al. [59] observed that as the Ag content increase, the amount of absorbed oxygen is accordingly increased, and this increase of absorbed oxygen causes leakage of oxygen-vacancies which strenuous the path of electrons from the valance band; VB to the conduction band; CB[59]. When the concentration of oxygen vacancies is decreased, impurity states become less delocalized and this leads to an increase in the composite bandgap [54].

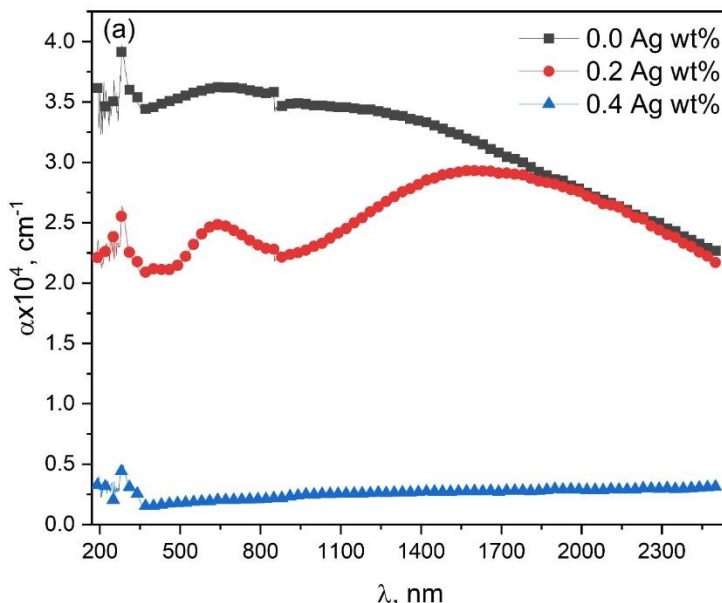
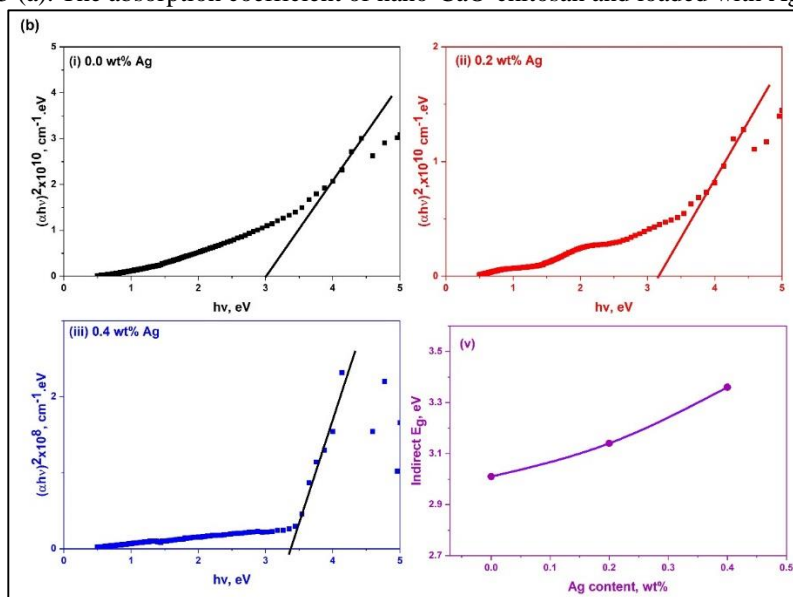


Fig. 5 (a). The absorption coefficient of nano-CaO-chitosan and loaded with Ag-NPs.



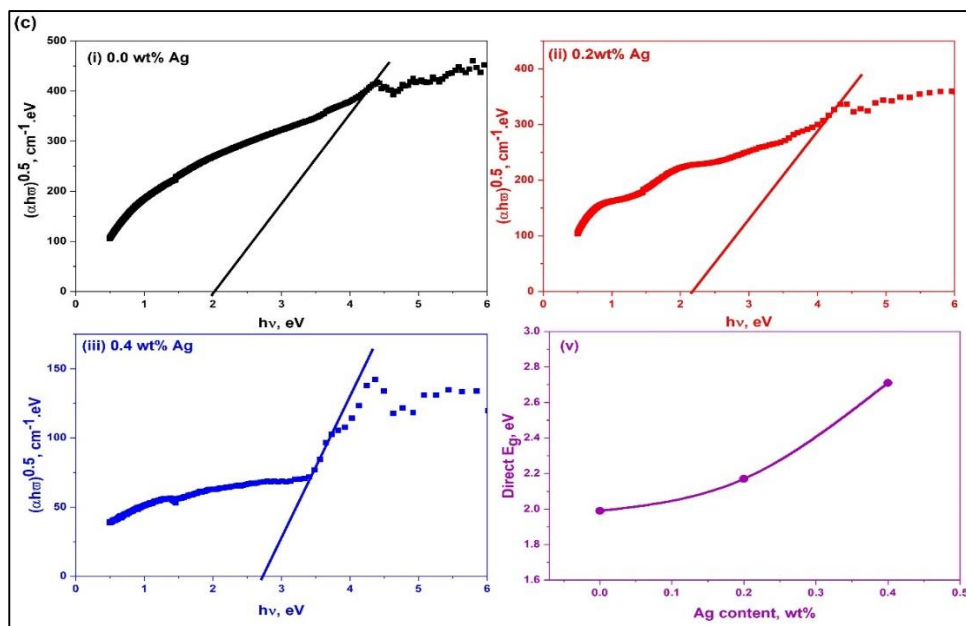


Fig. 5. (b) Indirect and (c) direct gap transition of nano-CaO-chitosan and loaded with (i) 0.0 wt.%, (ii) 0.2 wt.%, and (iii) 0.4 wt.% Ag, respectively. (v) shows the change of bandgap energy with Ag content.

Tauc's extrapolation technique is used to quantify the energy bandgap. The absorption coefficient is related to the energy band gap by Tauc's relation defined as [60]:

$$(\alpha h\nu) = B(h\nu - E_g)^a$$

Here, B is a constant factor, a is an index that defines the origin of the electronic change accounting for optical absorption whereas direct or indirect (1/2 and 2), $h\nu$ is the photon energy, and E_g is the optical band gap, and $h\nu$ is the light energy [61].

Also, Fig. 5 (b, c) indicates that the prepared nanocomposites undergo both direct and indirect gap

transition and the direct type is the more probable type [62, 63].

As a result of the bandgap increase with Ag addition, the optical conductivity (or the photoconductivity) of the nanocomposites shows a decreasing behavior as represented in Fig. 6.

The refractive index, n , shows no change with wavelength increase as in Fig. 7. Also, the figure shows a slight increase of refractive index with Ag addition.

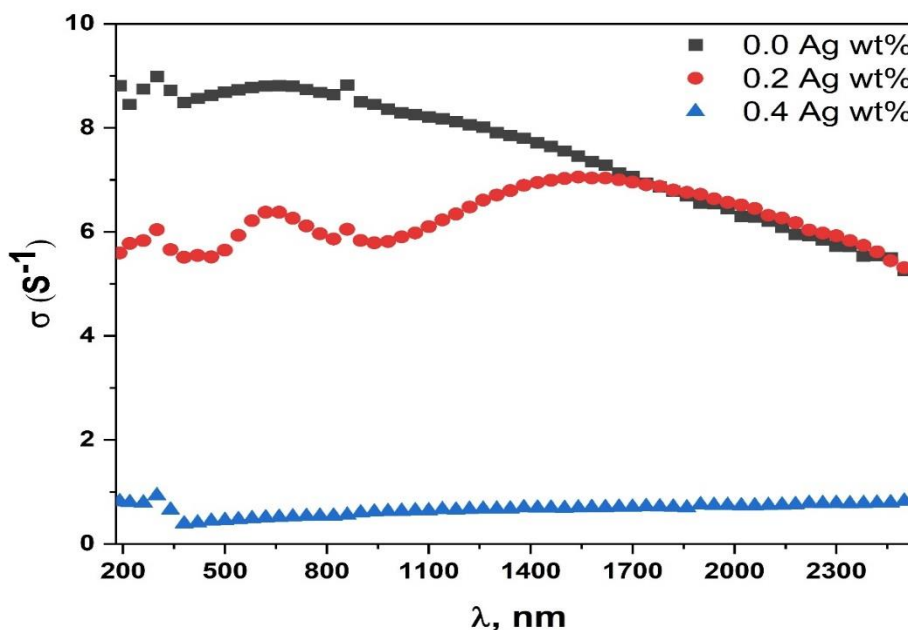


Fig. 6. Photoconductivity spectra of nano-CaO-chitosan and loaded with Ag-NPs.

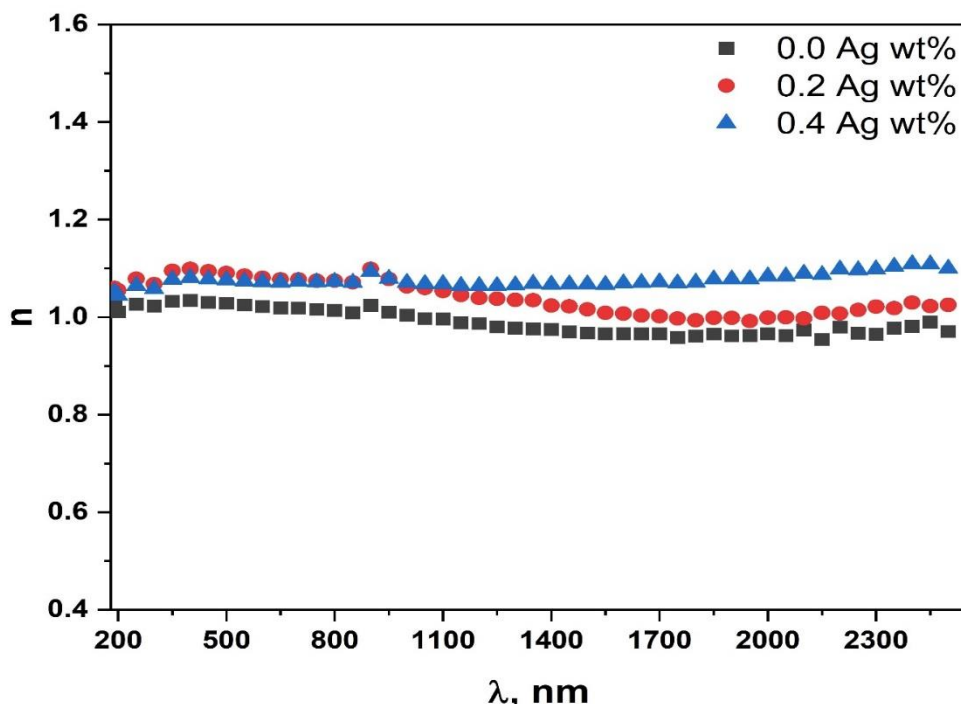


Fig. 7. Refractive indices of nano-CaO-chitosan and loaded with different concentrations of Ag-NPs.

3.5. Bacterial sensitivity of Ag/Ca chitosan nanocomposites

Table (1) presents the clearing inhibition zoon caused by Ag/Ca chitosan nanocomposite. The diameters zone around samples (CS, CS/Ca 0.2 Ag, CS/ Ca 0.4 Ag AndCS/ Ca 0.6 Ag) are:- (10, 11, 13 and 14 mm) for Staphylococcus aureus, (13, 12, 15 and 14 mm) for Pseudomonas aeruginosa, (9, 10, 11 and 10 mm) for Candida albicans and (2, 3, 2 and 2 mm) for Aspergillusniger.

The table demonstrates the inhibition zones that resulted in the agar plate later 24 h. The formed diameters of the inhibition zones were changes with Ag contents in the nano-CaO/Ag-chitosan nanocomposites. The antimicrobial activity of the synthesized Ag/Ca chitosan nanocomposite was

confirmed by the presence of a clear inhibition zone appears around the sample, in which consequently the pathogenic microorganisms were attacked by nanoparticles and enhanced the antimicrobial activity against different microbial species. Generally, the influence of the samples on the (*gram-positive, gram-negative*) bacteria and *fungus species* is comparable in terms of Ag/Ca chitosan nanocomposite samples. Substantially, for Ag/Ca chitosan samples, the increase in Ag/Ca concentration lead to an increase in the clearing inhibition zone around samples, while the clearing inhibition zone was slightly decreased in (CS/ Ca 0.6 Ag) sample which has the maximum concentration of Ag/Ca. This behavior was mainly attributed to the resistance feedback mechanism formed by microorganisms against the Ag/Ca after a certain concentration.

Table (1): Bacterial sensitivity of Ag/Ca chitosan nanocomposite.

Sample	zone (φmm)			
	Staphylococcus aureus	Pseudomonas aeruginosa	Candida albicans	Aspergillusniger
CS	10	13	9	2
CS/Ca 0.2 Ag	11	12	10	3
CS/ Ca 0.4 Ag	13	15	11	2
CS/ Ca 0.6 Ag	14	14	10	2

Chitosan is a linear polysaccharide consist mainly of randomly distributed poly(b-1-4)-2-amino-2-deoxy-D-glucopyranose, and it can be earned from the deacetylation process of chitin. Each glucosamine

monomer has amine and two hydroxyl groups act as active functional sites. Therefore chitosan is considered as a natural biopolymer that possesses good antimicrobial performance versus many

microorganisms such as Gram-positive and Gram-negative bacteria, fungi, and yeast. Many modifications such as physical and chemical modifications can be carried out to chitosan to increase its antimicrobial performance. Various possibilities responsible for antimicrobial activities have been recommended for chitosan, from junction to bacterial DNA which results in an inhibition of mRNA, to interact with surface molecules [64, 65]. A different hypothesis suggests that chitosan adheres to the membrane of bacteria and perturb it [66]. Several mechanisms responsible for antimicrobial activities have proposed but the most acceptable one is that the polycationic constitution of chitosan is owing to the occupancy of amine groups presented in glucosamine and might be a key feature to its capability to associate with negatively charged surface components of various microorganisms, making large changes to the cell exterior, reaching to damage of intracellular substances which cause cell death [67]. M Mesgari et al reported that the composition of chitosan and metallic nanoparticles (Titanium dioxide) can be utilized as a functional approach in antimicrobial packaging systems [68]. C. López-Badillo et al reported that CaO nanoparticles doped with Ag at different concentrations can increase the antimicrobial activity of the CaO nanoparticles toward *S. aureus* and *E. coli* for Growth kinetics [69]. S Mallakpour and M Okhovat synthesis a set of biocompatible nanocomposites composed of hydroxyapatite, chitosan, and tragacanth gum with different percentages of ZnO NPs and ZnO Ag NPs as fillers into the chitosan and tragacanth gum blend. they aimed to evaluate the antibacterial activity of these composite against *Staphylococcus aureus* and *Escherichia coli* bacteria. Commonly, the antibacterial activity of the biocompatible nanocomposites including ZnO/Ag NPs is more major than that containing ZnO NPs [70].

Conclusions

A successful study on the nano-CaO–chitosan and nano-CaO/Ag–chitosan nanocomposites have been made that are resulting from the acetic sol-gel process and polymerization. The Ag NPs concentration leverages on these nanocomposites are accomplished and their configurations are also characterized based on XRD, TEM, and FE-SEM techniques. The prepared nanocomposites undergo both direct and indirect gap transition and the direct type is the more probable type. The indirect energy gaps values were 3.01, 3.14, and 3.36 eV, and the direct energy gap values were 1.99, 2.17, and 2.71 eV for 0, 0.2, and 0.4 Ag⁺ loading, respectively. The refractive index has a value of about 1-1.1 with nearly no change with the wavelength change. A slight increase of refractive index with Ag addition was observed. Antimicrobial

assay and clearing inhibition zone around Ag/Ca chitosan samples shows the influence of the synthesized samples against the growth of various pathogenic microorganisms such as (*Staphylococcus aureus*) as a model of Gram-positive Bacteria, (*Pseudomonas aeruginosa*) as a model of Gram-negative Bacteria and (*Candida albicans* and *Aspergillusniger*) as models of fungal species. Antimicrobial assay results confirmed that the sample (CS/ Ca 0.4 Ag) from the prepared Ag/Ca chitosan nanocomposite samples can be used successfully as an Antimicrobial agent.

References

1. Cai, Y., Wu, D., Zhu, X., Wang, W., Tan, F., Chen, J., Qiao, X., Qiu, X.: Sol-gel preparation of Ag-doped MgO nanoparticles with high efficiency for bacterial inactivation. *Ceram. Int.* 43, 1066–1072 (2017). <https://doi.org/10.1016/j.ceramint.2016.10.041>.
2. Saber, S., Mollar, M., El Nahrawy, A., Khattab, N., Eid, A., Abo-Aly, M., Marí, B.: Annealing study of electrodeposited CuInSe₂ and CuInS₂ thin films. *Opt. Quantum Electron.* 50, (2018). <https://doi.org/10.1007/s11082-018-1521-1>.
3. El Nahrawy, A.M., Ali, A.I., Abou Hammad, A.B., Mbarek, A.: Structural and Optical Properties of Wet-chemistry Cu co-doped ZnTiO₃ Thin Films Deposited by Spin Coating Method. *Egypt. J. Chem.* 61, 1073–1081 (2018). <https://doi.org/10.21608/ejchem.2018.4069.1359>.
4. El Nahrawy, A.M., Abou Hammad, A.B., Bakr, A.M., Shaheen, T.I., Mansour, A.M.: Sol-gel synthesis and physical characterization of high impact polystyrene nanocomposites based on Fe₂O₃ doped with ZnO. *Appl. Phys. A Mater. Sci. Process.* 126, 654 (2020). <https://doi.org/10.1007/s00339-020-03822-w>.
5. Azab, A.A., Mansour, A.M., Turkey, G.M.: Structural, Magnetic, and Dielectric properties of Sr₄Fe₆O₁₃ ferrite prepared of small crystallites. *Sci. Rep.* 10, (2020). <https://doi.org/10.1038/s41598-020-61460-x>.
6. El Nahrawy, A.M., Hammad, A.B.A., Youssef, A.M., Mansour, A.M., Othman, A.M.: Thermal, dielectric and antimicrobial properties of polystyrene-assisted/ITO:Cu nanocomposites. *Appl. Phys. A Mater. Sci. Process.* 125, 1–9 (2019). <https://doi.org/10.1007/s00339-018-2351-5>.
7. Kamel, S., Haroun, A.A., El-Nahrawy, A.M., Diab, M.A.: Electroconductive composites containing nanocellulose, nanopolypyrrole, and silver nanoparticles. *J. Renew. Mater.* 7, 193–203 (2019).

- <https://doi.org/10.32604/jrm.2019.00144>.
8. Yin, D., Liu, J., Bo, X., Li, M., Guo, L.: Porphyrinic metal-organic framework/macroporous carbon composites for electrocatalytic applications. *Electrochim. Acta.* 247, 41–49 (2017). <https://doi.org/10.1016/j.electacta.2017.06.176>.
 9. El Nahrawy, A.M., Abou Hammad, A.B., Abdel-Aziz, M.S., Wassel, A.R.: Spectroscopic and Antimicrobial Activity of Hybrid Chitosan/Silica Membranes doped with Al₂O₃ Nanoparticles. *Silicon.* 11, (2019). <https://doi.org/10.1007/s12633-018-9986-x>.
 10. El Nahrawy, A.M., Hemdan, B.A., Abou Hammad, A.B., Abia, A.L.K., Bakr, A.M.: Microstructure and Antimicrobial Properties of Bioactive Cobalt Co-Doped Copper Aluminosilicate Nanocrystallines. *Silicon.* 12, 2317–2327 (2020). <https://doi.org/10.1007/s12633-019-00326-y>.
 11. Abou Hammad, A.B., Hemdan, B.A., El Nahrawy, A.M.: Facile synthesis and potential application of Ni_{0.6}Zn_{0.4}Fe₂O₄ and Ni_{0.6}Zn_{0.2}Ce_{0.2}Fe₂O₄ magnetic nanocubes as a new strategy in sewage treatment. *J. Environ. Manage.* 270, 110816 (2020). <https://doi.org/10.1016/j.jenvman.2020.110816>.
 12. Ashebir, M.E., Tesfamariam, G.M., Nigussie, G.Y., Gebreab, T.W.: Structural, optical, and photocatalytic activities of Ag-Doped and Mn-Doped ZnO Nanoparticles. *J. Nanomater.* 2018, (2018). <https://doi.org/10.1155/2018/9425938>.
 13. Hammad, A.B.A., El Nahrawy, A.M., Atia, D.M., El-Madany, H.T., Mansour, A.M.: Effect of Cu co-doping on the microstructure and optical properties of alumino-zinc thin films for optoelectronic applications. *Int. J. Mater. Eng. Innov.* 12, 18–36 (2021). <https://doi.org/10.1504/IJMATEI.2021.113214>.
 14. Mansour, A.M., Abou Hammad, A.B., El Nahrawy, A.M.: Sol-gel synthesis and physical characterization of novel MgCrO₄-MgCu₂O₃ layered films and MgCrO₄-MgCu₂O₃/p-Si based photodiode. *Nano-Structures and Nano-Objects.* 25, (2021). <https://doi.org/10.1016/j.nanoso.2020.100646>.
 15. El Nahrawy, A.M., Mansour, A.M., Abou Hammad, A.B.: Spectroscopic Study of Eu³⁺-Doped Magnesium Lanthanum Phosphate (MLPO) Films on SiO₂ Substrate. *Silicon.* (2021). <https://doi.org/10.1007/s12633-020-00855-x>.
 16. Tavízon-Pozos, J.A., Chavez-Esquivel, G., Suárez-Toriello, V.A., Santolalla-Vargas, C.E., Luévano-Rivas, O.A., Valdés-Martínez, O.U., Talavera-López, A., Rodríguez, J.A.: State of art of alkaline earth metal oxides catalysts used in the transesterification of oils for biodiesel production. *Energies.* 14, 1031 (2021). <https://doi.org/10.3390/en14041031>.
 17. Das, M.C., Xiang, S., Zhang, Z., Chen, B.: Functional mixed metal-organic frameworks with metalloligands, (2011). <https://doi.org/10.1002/anie.201101534>.
 18. El Nahrawy, A.M., Mansour, A.M., Abou Hammad, A.B., Ibrahim, R.S., Abouelnaga, A.M., Abdel-Aziz, M.S.: Optical, Functional Impact and Antimicrobial of Chitosan/Phosphosilicate/Al₂O₃ Nanosheets. *J. Inorg. Organomet. Polym. Mater.* 30, 3084–3094 (2020). <https://doi.org/10.1007/s10904-020-01469-x>.
 19. Youssef, A.M., El-Nahrawy, A.M., Abou Hammad, A.B.: Sol-gel synthesis and characterizations of hybrid chitosan-PEG/calcium silicate nanocomposite modified with ZnO-NPs and (E102) for optical and antibacterial applications. *Int. J. Biol. Macromol.* 97, 561–567 (2017). <https://doi.org/10.1016/J.IJBIOMAC.2017.01.059>.
 20. Wu, J.J., Tseng, C.H.: Photocatalytic properties of nc-Au/ZnO nanorod composites. *Appl. Catal. B Environ.* 66, 51–57 (2006). <https://doi.org/10.1016/j.apcatb.2006.02.013>.
 21. Garcia, M.A.: Surface plasmons in metallic nanoparticles: Fundamentals and applications, <https://iopscience.iop.org/article/10.1088/0022-3727/44/28/283001>, (2011). <https://doi.org/10.1088/0022-3727/44/28/283001>.
 22. Deshmukh, S.P., Dhokale, R.K., Yadav, H.M., Achary, S.N., Delekar, S.D.: Titania-supported silver nanoparticles: An efficient and reusable catalyst for reduction of 4-nitrophenol. *Appl. Surf. Sci.* 273, 676–683 (2013). <https://doi.org/10.1016/j.apsusc.2013.02.110>.
 23. Chao, H.E., Yun, Y.U., Xingfang, H.U., Larbot, A.: Effect of silver doping on the phase transformation and grain growth of sol-gel titania powder. *J. Eur. Ceram. Soc.* 23, 1457–1464 (2003). [https://doi.org/10.1016/S0955-2219\(02\)00356-4](https://doi.org/10.1016/S0955-2219(02)00356-4).
 24. Krishna Sailaja, A., Amareshwar, P., Chakravarty, P.: Chitosan nanoparticles as a drug delivery system, (2010).
 25. El Nahrawy, A.M., Mansour, A.M., Abou Hammad, A.B., Ibrahim, R.S., Abouelnaga, A.M., Abdel-Aziz, M.S.: Optical, Functional Impact and Antimicrobial of Chitosan/Phosphosilicate/Al₂O₃ Nanosheets. *J. Inorg. Organomet. Polym. Mater.* 30, 3084–3094 (2020). <https://doi.org/10.1007/s10904-020-01469-x>.
 26. Elnahrawy, A.M., Kim, Y.S., Ali, A.I.: Synthesis

- of hybrid chitosan/calcium aluminosilicate using a sol-gel method for optical applications. *J. Alloys Compd.* 676, 432–439 (2016). <https://doi.org/10.1016/j.jallcom.2016.03.210>.
27. Abou Hammad, A.B., Elnahrawy, A.M., Youssef, A.M., Youssef, A.M.: Sol gel synthesis of hybrid chitosan/calcium aluminosilicate nanocomposite membranes and its application as support for CO₂ sensor. *Int. J. Biol. Macromol.* 125, 503–509 (2019). <https://doi.org/10.1016/j.ijbiomac.2018.12.077>.
 28. Tai, A., Sawano, T., Yazama, F., Ito, H.: Evaluation of antioxidant activity of vanillin by using multiple antioxidant assays. *Biochim. Biophys. Acta - Gen. Subj.* 1810, 170–177 (2011). <https://doi.org/10.1016/j.bbagen.2010.11.004>.
 29. Tao, Y., Zhang, H.L., Hu, Y.M., Wan, S., Su, Z.Q.: Preparation of chitosan and water-soluble chitosan microspheres via spray-drying method to lower blood lipids in rats fed with high-fat diets. *Int. J. Mol. Sci.* 14, 4174–4184 (2013). <https://doi.org/10.3390/ijms14024174>.
 30. ElNahrawy, A.M., Mansour, A.M., ElAttar, H.A., Sakr, E.M.M., Soliman, A.A., Hammad, A.B.A.: Impact of Mn-substitution on structural, optical, and magnetic properties evolution of sodium-cobalt ferrite for opto-magnetic applications. *J. Mater. Sci. Mater. Electron.* 31, 6224–6232 (2020). <https://doi.org/10.1007/s10854-020-03176-2>.
 31. Higazy, A.A., Afifi, H., Khafagy, A.H., El-Shahawy, M.A., Mansour, A.M.: Ultrasonic studies on polystyrene/styrene butadiene rubber polymer blends filled with glass fiber and talc. *Ultrasonics* 44, (2006). <https://doi.org/10.1016/j.ultras.2006.05.142>.
 32. Pradhan, A.K., Sahoo, P.K.: Synthesis and study of thermal, mechanical and biodegradation properties of chitosan-g-PMMA with chicken egg shell (nano-CaO) as a novel bio-filler. *Mater. Sci. Eng. C.* 80, 149–155 (2017). <https://doi.org/10.1016/j.msec.2017.04.076>.
 33. El Nahrawy, A.M., Bakr, A.M., Abou Hammad, A.B., Hemdan, B.A.: High performance of talented copper/magneso-zinc titanate nanostructures as biocidal agents for inactivation of pathogens during wastewater disinfection. *Appl. Nanosci.* 10, 3585–3601 (2020). <https://doi.org/10.1007/s13204-020-01454-3>.
 34. Xiao, G., Zhang, X., Zhang, W., Zhang, S., Su, H., Tan, T.: Visible-light-mediated synergistic photocatalytic antimicrobial effects and mechanism of Ag-nanoparticles@chitosan-TiO₂ organic-inorganic composites for water disinfection. *Appl. Catal. B Environ.* 170–171, 255–262 (2015). <https://doi.org/10.1016/j.apcatb.2015.01.042>.
 35. Al-esnawy, A.A., Ereiba, K.T., Bakr, A.M., Abdraboh, A.S.: Characterization and antibacterial activity of Streptomycin Sulfate loaded Bioglass/Chitosan beads for bone tissue engineering. *J. Mol. Struct.* 1227, (2021). <https://doi.org/10.1016/j.molstruc.2020.129715>.
 36. Abou Hammad, A.B., Bakr, A.M., Abdel-Aziz, M.S., El Nahrawy, A.M.: Exploring the ferroelectric effect of nanocrystalline strontium zinc titanate/Cu: Raman and antimicrobial activity. *J. Mater. Sci. Mater. Electron.* 31, 7850–7861 (2020). <https://doi.org/10.1007/s10854-020-03323-9>.
 37. El Nahrawy, A.M., Bakr, A.M., Hemdan, B.A., Abou Hammad, A.B.: Identification of Fe³⁺ co-doped zinc titanate mesostructures using dielectric and antimicrobial activities. *Int. J. Environ. Sci. Technol.* 17, 4481–4494 (2020). <https://doi.org/10.1007/s13762-020-02786-x>.
 38. El Nahrawy, A.M., Abou Hammad, A.B., Mansour, A.M.: Preparation and Characterization of Transparent Semiconducting Silica Nanocomposites Doped with P₂O₅ and Al₂O₃. *Silicon* (2021). <https://doi.org/10.1007/s12633-021-00962-3>.
 39. El Nahrawy, A.M., Hemdan, B.A., Abou Hammad, A.B., Othman, A.M., Abouelnaga, A.M., Mansour, A.M.: Modern Template Design and Biological Evaluation of Cephadrine-loaded Magnesium Calcium Silicate Nanocomposites as an Inhibitor for Nosocomial Bacteria in Biomedical Applications. *Silicon*. in press, (2020). <https://doi.org/10.1007/s12633-020-00642-8>.
 40. Abou Hammad, A.B., El Nahrawy, A.M., Hemdan, B.A., Abia, A.L.K.: Nanoceramics and novel functionalized silicate-based magnetic nanocomposites as substitutional disinfectants for water and wastewater purification. *Environ. Sci. Pollut. Res.* 27, 26668–26680 (2020). <https://doi.org/10.1007/s11356-020-09073-9>.
 41. Abouelnaga, A.M., Meaz, T.M., Othman, A.M., Ghazy, R.A., El Nahrawy, A.M.: Probing the Structural and Antimicrobial Study on a Sol-Gel Derived Velosef-Loaded Bioactive Calcium Magneso-Silicate Xerogel. *Silicon* 13, 623–631 (2021). <https://doi.org/10.1007/s12633-020-00448-8>.
 42. Hussain, N.S., Lopes, M.A., Santos, J.D.: A comparative study of CaO-P₂O₅-SiO₂ gels prepared by a sol-gel method. *Mater. Chem. Phys.* 88, 5–8 (2004). <https://doi.org/10.1016/j.matchemphys.2004.06.015>.
 43. Dong, F., Guo, S., Wang, H., Li, X., Wu, Z.: Enhancement of the visible light photocatalytic

- activity of C-doped TiO₂ nanomaterials prepared by a green synthetic approach. *J. Phys. Chem. C*. 115, 13285–13292 (2011). <https://doi.org/10.1021/jp111916q>.
44. Shao, Y., Cao, C., Chen, S., He, M., Fang, J., Chen, J., Li, X., Li, D.: Investigation of nitrogen doped and carbon species decorated TiO₂ with enhanced visible light photocatalytic activity by using chitosan. *Appl. Catal. B Environ.* 179, 344–351 (2015). <https://doi.org/10.1016/j.apcatb.2015.05.023>.
 45. Chen, C., Hu, Y., Zhu, H., Sun, W., Qin, W., Liu, R., Gao, Z.: Inhibition performance and adsorption of polycarboxylic acids in calcite flotation. *Miner. Eng.* 133, 60–68 (2019). <https://doi.org/10.1016/j.mineng.2018.12.027>.
 46. Ahn, J.S., Choi, H.K., Cho, C.S.: A novel mucoadhesive polymer prepared by template polymerization of acrylic acid in the presence of chitosan. *Biomaterials*. 22, 923–928 (2001). [https://doi.org/10.1016/S0142-9612\(00\)00256-8](https://doi.org/10.1016/S0142-9612(00)00256-8).
 47. Koev, S.T., Dykstra, P.H., Luo, X., Rubloff, G.W., Bentley, W.E., Payne, G.F., Ghodssi, R.: Chitosan: An integrative biomaterial for lab-on-a-chip devices, (2010). <https://doi.org/10.1039/c0lc00047g>.
 48. Ponnamma, D., Sadasivuni, K.K., AlMaadeed, M.A.: Introduction of Biopolymer Composites: What to do in Electronics? In: *Biopolymer Composites in Electronics*. pp. 1–12. Elsevier Inc. (2017). <https://doi.org/10.1016/B978-0-12-809261-3.00001-2>.
 49. Patel, G.B., Singh, N.L., Singh, F., Kulriya, P.K.: Effect of swift heavy ions irradiation on physicochemical and dielectric properties of chitosan and chitosan-Ag nanocomposites. *Radiat. Phys. Chem.* 181, 109288 (2021). <https://doi.org/10.1016/j.radphyschem.2020.109288>.
 50. Patel, G.B., Singh, N.L., Singh, F.: Modification of chitosan-based biodegradable polymer by irradiation with MeV ions for electrolyte applications. *Mater. Sci. Eng. B Solid-State Mater. Adv. Technol.* 225, 150–159 (2017). <https://doi.org/10.1016/j.mseb.2017.08.023>.
 51. Farag, A.A.M., Terra, F.S., Mahmoud, G.M., Mansour, A.M.: Study of Gaussian distribution of inhomogeneous barrier height for n-InSb/p-GaAs heterojunction prepared by flash evaporation. *J. Alloys Compd.* 481, 427–433 (2009). <https://doi.org/10.1016/j.jallcom.2009.03.004>.
 52. Farag, A.A.M., Mansour, A.M., Ammar, A.H., Rafea, M.A.: Characterization of electrical and optical absorption of organic based methyl orange for photovoltaic application. *Synth. Met.* 161, 2135–2143 (2011). <https://doi.org/10.1016/j.synthmet.2011.08.015>.
 53. Farag, A.A.M., Osiris, W.G., Ammar, A.H., Mansour, A.M.: Electrical and photosensing performance of heterojunction device based on organic thin film structure. *Synth. Met.* 175, 81–87 (2013). <https://doi.org/10.1016/j.synthmet.2013.04.030>.
 54. Singh, R., Barman, P.B., Sharma, D.: Synthesis, structural and optical properties of Ag doped ZnO nanoparticles with enhanced photocatalytic properties by photo degradation of organic dyes. *J. Mater. Sci. Mater. Electron.* 28, 5705–5717 (2017). <https://doi.org/10.1007/s10854-016-6242-2>.
 55. Hassan, N., Mansour, A.M., Roushdy, N., Farag, A.A.M., Osiris, W.G.: Optical sensing performance characteristics of Schottky devices diodes based nano-particle disodium 6-hydroxy-5-[(2-methoxy-5-methyl-4-sulfophenyl)azo]-2-naphthalenesulfonate thin films: A comparison study. *Optik (Stuttg.)*. 158, 1255–1265 (2018). <https://doi.org/10.1016/j.ijleo.2017.12.203>.
 56. Mansour, A.M., El Radaf, I.M.: Structural, optical and electrical properties of CuBiS₂ thin films deposited by spray pyrolysis at different deposition times. *Int. J. Microstruct. Mater. Prop.* 14, 419–431 (2019). <https://doi.org/10.1504/IJMMP.2019.102219>.
 57. Jin, Y., Cui, Q., Wang, K., Hao, J., Wang, Q., Zhang, J.: Investigation of photoluminescence in undoped and Ag-doped ZnO flowerlike nanocrystals. *J. Appl. Phys.* 109, (2011). <https://doi.org/10.1063/1.3549826>.
 58. Lv, H., Sang, D.D., Li, H.D., Du, X.B., Li, D.M., Zou, G.T.: Thermal evaporation synthesis and properties of ZnO nano/microstructures using carbon group elements as the reducing agents. *Nanoscale Res. Lett.* 5, 620–624 (2010). <https://doi.org/10.1007/s11671-010-9524-2>.
 59. López-Badillo, C.M., Hernández-González, M., Hernández-Centeno, F., Olivas-Armendáriz, I., Rodríguez-González, C.A., Múzquiz-Ramos, E.M., López-Cuevas, J., López-De la Peña, H.Y.: Antibacterial activity and in vitro cytotoxicity studies of Ag-doped CaO nanoparticles. *Mater. Lett.* 283, (2021). <https://doi.org/10.1016/j.matlet.2020.128741>.
 60. El Nahrawy, A.M., Mansour, A.M., Abou Hammad, A.B., Wassel, A.R.: Effect of Cu incorporation on morphology and optical band gap properties of nano-porous lithium magnesio-silicate (LMS) thin films. *Mater. Res. Express.* 6, 016404 (2019). <https://doi.org/10.1088/2053-1591/aae343>.
 61. Mansour, A.M., El Radaf, I.M., Mahmoud, G.M.: Effect of deposition temperature on structural, optical and electrical properties of chemically deposited thermochromic Cu₂HgI₄

- thin films. *Int. J. Microstruct. Mater. Prop.* 14, 462–477 (2019).
<https://doi.org/10.1504/IJMMP.2019.102223>.
62. Mansour, A.M.: Fabrication and Characterization of a Photodiode Based on 5',5"-dibromo-o-cresolsulphophthalein (BCP). *Silicon* 11, 1989–1996 (2019).
<https://doi.org/10.1007/s12633-018-0016-9>.
63. Mansour, A.M., Nasr, M., Saleh, H.A., Mahmoud, G.M.: Physical characterization of 5',5"-dibromo-o-cresolsulphophthalein (BCP) spin-coated thin films and BCP/p-Si based diode. *Appl. Phys. A Mater. Sci. Process.* 125, (2019). <https://doi.org/10.1007/s00339-019-2920-2>.
64. Goy, R.C., De Britto, D., Assis, O.B.G.: A review of the antimicrobial activity of chitosan, (2009). <https://doi.org/10.1590/S0104-14282009000300013>.
65. Hosseinnajad, M., Jafari, S.M.: Evaluation of different factors affecting antimicrobial properties of chitosan, (2016). <https://doi.org/10.1016/j.ijbiomac.2016.01.022>.
66. Raafat, D., Sahl, H.G.: Chitosan and its antimicrobial potential - A critical literature survey, /pmc/articles/PMC3815839/, (2009). <https://doi.org/10.1111/j.1751-7915.2008.00080.x>.
67. Ganan, M., Carrascosa, A. V., Martínez-Rodríguez, A.J.: Antimicrobial activity of chitosan against campylobacter spp. and other microorganisms and its mechanism of action. *J. Food Prot.* 72, 1735–1738 (2009). <https://doi.org/10.4315/0362-028x-72.8.1735>.
68. Mesgari, M., Aalami, A.H., Sahebkar, A.: Antimicrobial activities of chitosan/titanium dioxide composites as a biological nanolayer for food preservation: A review, (2021). <https://doi.org/10.1016/j.ijbiomac.2021.02.099>.
69. López-Badillo, C.M., Hernández-González, M., Hernández-Centeno, F., Olivas-Armendáriz, I., Rodríguez-González, C.A., Múzquiz-Ramos, E.M., López-Cuevas, J., López-De la Peña, H.Y.: Antibacterial activity and in vitro cytotoxicity studies of Ag-doped CaO nanoparticles. *Mater. Lett.* 283, 128741 (2021). <https://doi.org/10.1016/j.matlet.2020.128741>.
70. Mallakpour, S., Okhovat, M.: Hydroxyapatite mineralization of chitosan-tragacanth blend/ZnO/Ag nanocomposite films with enhanced antibacterial activity. *Int. J. Biol. Macromol.* 175, 330–340 (2021). <https://doi.org/10.1016/j.ijbiomac.2021.01.210>.